

# Radio Pulsating Structures with Coronal Loop Contraction

J. Kallunki · S. Pohjolainen

Received: 15 November 2011 / Accepted: 18 April 2012  
© Springer Science+Business Media B.V. 2012

**Abstract** We present a multi-wavelength study of a solar eruption event on 20 July 2004, comprising observations in H $\alpha$ , EUV, soft X-rays, and in radio waves with a wide frequency range. The analyzed data show both oscillatory patterns and shock wave signatures during the impulsive phase of the flare. At the same time, large-scale EUV loops located above the active region were observed to contract. Quasi-periodic pulsations with  $\sim 10$  and  $\sim 15$  s oscillation periods were detected both in microwave–millimeter waves and in decimeter–meter waves. Our calculations show that MHD oscillations in the large EUV loops – but not likely in the largest contracting loops – could have produced the observed periodicity in radio emission, by triggering periodic magnetic reconnection and accelerating particles. As the plasma emission in decimeter–meter waves traces the accelerated particle beams and the microwave emission shows a typical gyrosynchrotron flux spectrum (emission created by trapped electrons within the flare loop), we find that the particles responsible for the two different types of emission could have been accelerated in the same process. Radio imaging of the pulsed decimetric–metric emission and the shock-generated radio type II burst in the same wavelength range suggest a rather complex scenario for the emission processes and locations. The observed locations cannot be explained by the standard model of flare loops with an erupting plasmoid located above them, driving a shock wave at the CME front.

**Keywords** Sun: flares · Coronal mass ejections (CMEs) · Oscillations · Radio radiation · Shock waves · Radiation mechanisms: non-thermal

---

Advances in European Solar Physics

Guest Editors: Valery M. Nakariakov, Manolis K. Georgoulis, and Stefaan Poedts

**Electronic supplementary material** The online version of this article (doi:[10.1007/s11207-012-0003-z](https://doi.org/10.1007/s11207-012-0003-z)) contains supplementary material, which is available to authorized users.

---

J. Kallunki

Metsähovi Radio Observatory, Aalto University, Kylmälä, Finland  
e-mail: [kallunki@kurp.hut.fi](mailto:kallunki@kurp.hut.fi)

S. Pohjolainen (✉)

Department of Physics and Astronomy, Tuorla Observatory, University of Turku, Piikkiö, Finland  
e-mail: [silpoh@utu.fi](mailto:silpoh@utu.fi)

## 1. Introduction

Coronal loop oscillations have in many cases been suggested to be the source of radio pulsations. Loop oscillations can either change the magnetic field strength within the loop or they can change the direction of the magnetic field, and thus modulate the radio flux (gyrosynchrotron emission mechanism) in microwaves and millimeter waves (Grechnev, White, and Kundu, 2003). Alternatively, the electron number density and/or electron energy distribution can change due to reconnection processes, causing periodic changes in the flux (Dulk, 1985). Decimetric – metric pulsations are generally considered as tracers of non-thermal electrons and their acceleration, and the suggested emission processes include instabilities (such as loss-cone instability) or plasma emission by beams (Benz, Battaglia, and Vilmer, 2011, and references therein). Recently, Nakariakov *et al.* (2006) proposed a mechanism where an oscillating loop situated nearby a flaring arcade is capable to leak oscillations to magnetic null points in the arcade, modulating the current density and triggering magnetic reconnection. The periodically accelerated particles follow the field lines and cause pulsations, which can be observed at several wavelengths. These may include the decimetric frequency range where drifting pulsating structures have been observed and interpreted as electron beams injected into the plasmoid during quasi-periodic reconnection processes (Karlicky, 2004).

Contracting motions in flaring loops during the rising phase of solar flares have been reported (*e.g.*, Ji, Huang, and Wang, 2007, and references therein). Contraction of overlying coronal loops in flaring active regions have also been observed. Liu, Wang, and Alexander (2009) suggested that a prolonged preheating period is necessary to explain the long and slow implosion phase before eruption. The formation of a shrinking trap was further proposed by Liu and Wang (2009) in the case where overlying coronal loops started to contract when the filament underneath erupted. The later-observed isolated hard X-ray burst was explained as the result of the contracting loops approaching the post-flare arcade. A collapsing magnetic trap and emission by trapped high-energy electrons was also suggested by Karlicky and Kosugi (2004), to explain the delayed decimetric radio emission. Most recently, coronal loop contraction has been suggested to be a new mechanism for coronal loop oscillations, to be caused by the contracting loops that interact with the loops located below (Liu and Wang, 2010). The produced oscillation periods would be in the ten-minute range.

In this paper we analyze a CME-related GOES M8.6 class flare that occurred in active region (AR) NOAA 10652 on 20 July 2004. During the flare, the coronal loops above the AR showed downward movement, visible in the SOHO/EIT images. This was interpreted as a possible coronal implosion event by Liu and Wang (2010). We now investigate the event further using  $H\alpha$ , EUV, soft X-ray, and radio imaging data, together with wide-range radio dynamic spectra and flux density observations in microwaves, as radio pulsating structures were observed during the flare impulsive phase. Our aim is to see if the observed radio pulsations were somehow associated with the collapsing coronal loop system. Section 2 describes the observations, Section 3 describes the analysis, and in Section 4 we summarize the results. Discussion and conclusions are presented in Section 5.

## 2. Observations

On 20 July 2004 the NOAA AR 10652 produced several flares and coronal mass ejections. The most intense flare was reported to start at 12:22 UT, located at N10 E35, reaching GOES class M8.6 at 12:32 UT. In  $H\alpha$ , the flare was reported to start at 12:26 UT. The flare was also associated with a filament eruption.

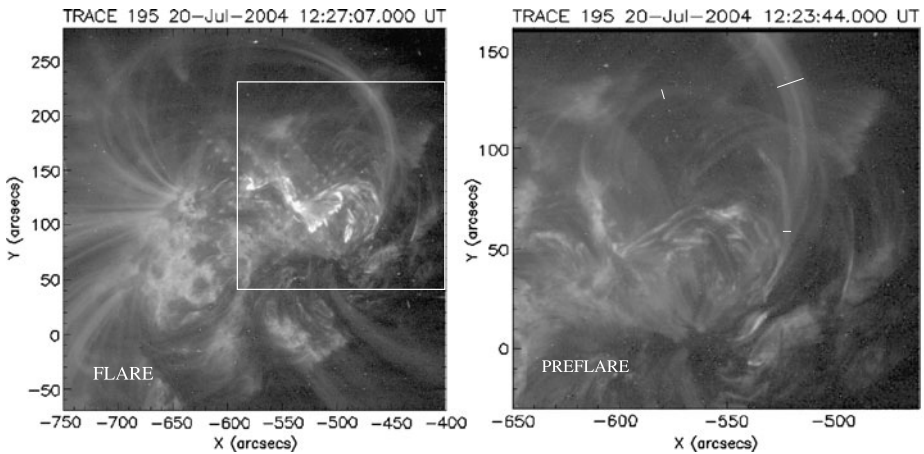


**Figure 1** Left: TRACE 195 Å image at 12:27:07 UT, during the flare impulsive phase and just after the decimetric and microwave pulsations had started. A two-ribbon flare was formed below the large EUV loop system. Right: A zoom of the active region at 12:23:44 UT, before the flare impulsive phase. The zoomed region is indicated in the 12:27:07 UT image with a box; note that the axis values are relative to the pointing and change between the frames. White lines in the 12:23:44 UT image mark the loop widths (see Section 3.2).

A halo-type coronal mass ejection was observed about one hour after the M8.6 flare maximum, propagating toward the north. The CME speed was relatively low, about  $500 \text{ km s}^{-1}$ , when first observed at 13:31–13:54 UT at heights 2.8–3.8  $R_{\odot}$ , but the CME was observed to accelerate later.

### 2.1. EUV, H $\alpha$ , and X-ray Structures

TRACE images at 195 Å wavelength before and at the flare start at 12:23 and 12:27 UT show an active region with overlying large-scale loops (Figure 1). The overlying EUV loops were later observed to contract (*i.e.*, they appeared to lose height and collapse) in the SOHO EIT difference images at 12:36 and 12:48 UT (Figure 2). The EIT image cadence was not high enough to follow the collapse in detail, but in the earlier EIT image at 12:24 UT no collapse is visible. The TRACE field-of-view is unfortunately too limited to see the loop movement, but the forming of a two-ribbon flare below the large EUV loop is well observed.

H $\alpha$  images (one-minute time cadence) from Kanzelhöhe Solar Observatory (Figure 3) show how bright patches appear north of the AR at 12:28:15 UT. One minute later more patches are visible more north. The distance between the outermost patches in the 12:28:15 and 12:29:15 UT images is about  $30''$ , indicating a speed of at least  $350 \text{ km s}^{-1}$  for a propagating disturbance.

GOES SXI full-disk observations in soft X-rays are available with two minute time cadence, and at 12:30 UT a dimming region appears north of the AR. In the next image at 12:32 the dimming region has become more wide and has propagated northward (Figure 4). The running difference image at 12:30 UT also shows a bright rim ahead of the dimming, suggesting it could be a wave-like structure. The locations of the outermost H $\alpha$  bright patches at 12:29:15 UT are marked in the 12:30 UT SXI difference image in Figure 4. The locations match with the SXI bright rim.

Hard X-ray observations of this event were very limited. Only the flare decay phase was observed by RHESSI during 12:35–12:45 UT. There is some indication of rising count rates

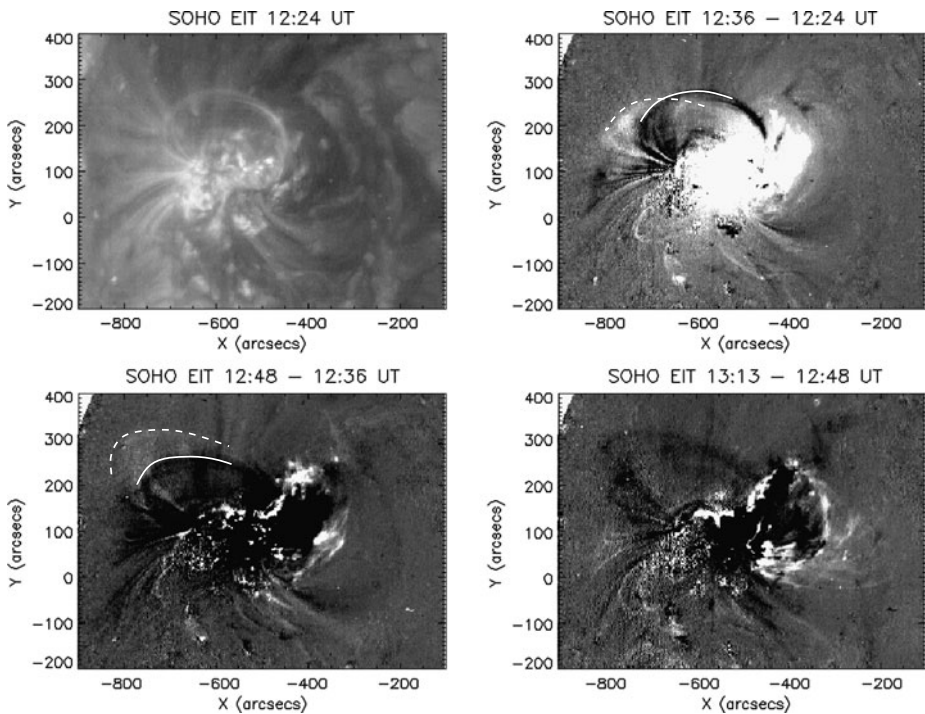


**Figure 2** SOHO EIT image of the flaring active region at 12:24 UT (top left), followed by EIT running difference images at 12:36, 12:48, and 13:13 UT. Solid and dashed lines outline the locations of the collapsing loops in temporal order, respectively, directed toward the north-east. The filament eruption, observed best in the last difference image at 13:13 UT, is directed toward the west. See also movie in the electronic version of this article, consisting of the EIT images between 12:00 and 13:48 UT.

at high energies after 12:42 UT, but observations were then cut due to satellite night time. A single hard X-ray emission source can be observed at  $x = -500''$ ,  $y = 125''$  from the disk center at 12:43:22 UT (RHESSI Browser and Archive data).

## 2.2. Radio Flux Densities and Spectral Structures

The solar eruption on 20 July 2004 was associated with radio emission at a wide frequency range, as shown in Figure 5. Millimeter and centimeter wave emission was recorded at 8.4, 11.8, 19.6, and 35.0 GHz (single frequency full-disk flux density observations at Bumishus). The burst maximum was observed at 12:28:55 UT at 19.6 GHz, and the flux density reached 13 100 sfu. The flux density spectra with a spectral turn-over frequency near 20 GHz indicates a typical gyrosynchrotron source. The relatively high turn-over frequency suggests high-energy electrons and/or high densities and magnetic field strengths.

At the time of start of the microwave emission at 8.4 GHz at 12:26 UT, decimetric pulsating structures appear in the dynamic spectrum in the 1.4–2.0 GHz frequency range (ETHZ *Phoenix-2*, Figure 5). The pulsating emission envelopes then drift toward the lower frequencies, indicating a source that moves to lower densities, *i.e.*, outward to larger heights. The decimetric pulsations were only mildly polarized and below 500 MHz the polarization data was not usable (private communication from Christian Monstein).

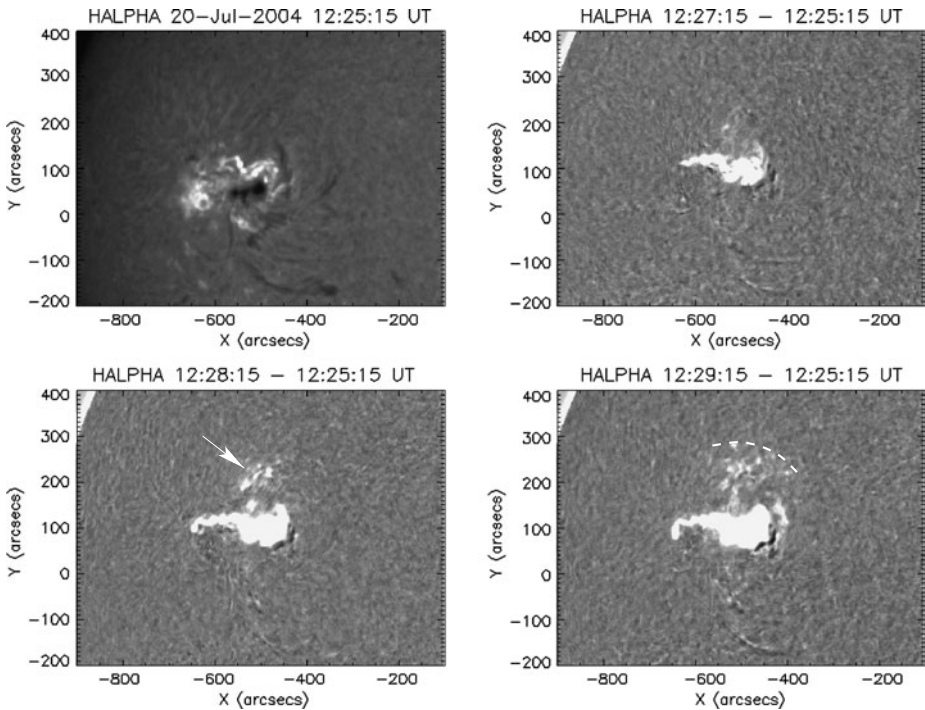


**Figure 3**  $H\alpha$  patrol observations from Kanzelhöhe Solar Observatory (Global High Resolution  $H\alpha$  Network). The first image shows the active region at 12:25:15 UT (used as the base image) and the next ones are the base differences at 12:27:15–12:29:15 UT. Bright regions appear north of the AR at 12:28:15 UT and one minute later the brightenings have propagated further. The outermost brightenings form an arc-like structure, indicated with a dashed line.

A metric radio type II burst was observed to form almost like a continuation of the pulsations, at a frequency of about 150 MHz (ETHZ *Phoenix-2* spectra). The GBSRBS observations at 70–20 MHz show two separate traces of fundamental–harmonic type II pairs simultaneously. The pairs show different drift rates and this could indicate either emission from two different locations (with different density gradients) within a large-scale shock or two separate, more localized shocks (White, 2007). The faster-drifting type II burst emission appears to form after 12:35 UT (fundamental harmonic–pair at 40 and 80 MHz). The slower-drifting metric burst emission may be a continuation of the pulsations burst lane imaged at 150 MHz at 12:31–12:32 UT. Note that there is a gap in the spectral data at 100–70 MHz.

At 12:32:40 UT a slowly drifting wide-band emission feature appears in the dynamic spectrum at about 800–900 MHz. ‘TS/F’ in Figures 5 and 6 point to a feature that could be caused by a termination shock (TS). Similar structures have been shown by, *e.g.*, Aurass and Mann (2004), where the two separate bands of slow-drifting features (not harmonically related) were interpreted as standing fast-mode shocks between the diffusion region and the top of the post-flare loops (lower TS, high-frequency emission band) and between the diffusion region and the erupting filament (upper TS, low frequency band).

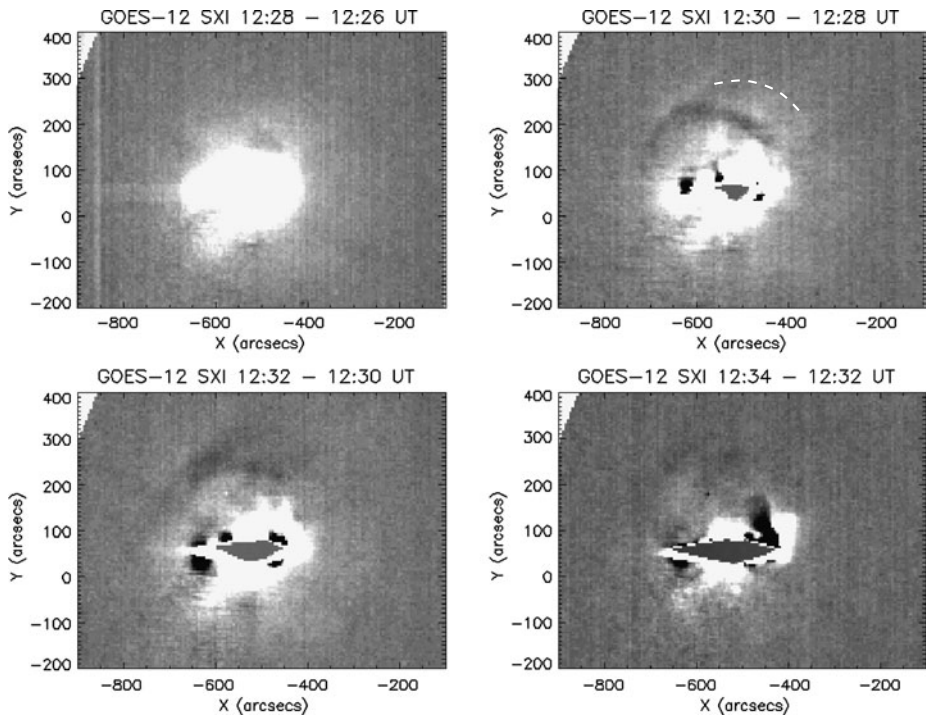


**Figure 4** GOES SXI soft X-ray running difference images between 12:28 and 12:34 UT, with two minute image cadence. A dimming region is observed to propagate toward the north, with a bright sector in front of it. Note that the pixels in the active region center have saturated. The dashed line in the 12:30 UT SXI running difference image marks the location of the arc of bright  $H\alpha$  patches at 12:19:15 UT.

### 2.3. Radio Imaging

Some of these spectral features were imaged at selected frequencies between 150 and 432 MHz by the *Nançay Radioheliograph*. The locations of the pulsating emission source centers during 12:29–12:31 UT are shown in Figure 6. These emission sources are located near the soft X-ray dimming region and the bright  $H\alpha$  patches, north of the AR.

Some of the pulsating structures are similar to type III burst groups, caused by beams of accelerated electrons, and some of them show clear frequency drifts toward the higher frequencies. As drifts to higher frequencies indicate increasing electron densities, it is assumed that the electron beams follow the magnetic field lines back to the Sun, to higher densities. The radio images of one of the bursts at 12:30 UT (Figure 7) show an almost horizontal burst trajectory toward the east. Due to projection effects we cannot determine the beam paths in detail, but the source locations suggest that the electrons could have been streaming along a (flat) large-scale loop top.

Soon after the 12:29–12:31 UT pulsating features a type II burst was formed. It is visible in the *Nançay* radio images at 150 MHz after 12:32:50 UT, located above the pulsating decimetric emission sources observed at 432 MHz (Figure 8).

The ‘TS/F’ feature shown in Figure 5 cannot be imaged at 800 MHz but the *Nançay Radioheliograph* images show burst emission also at  $\sim 400$  MHz. It could be a fundamental–harmonic pair but this complicates the termination shock interpretation, at least if we

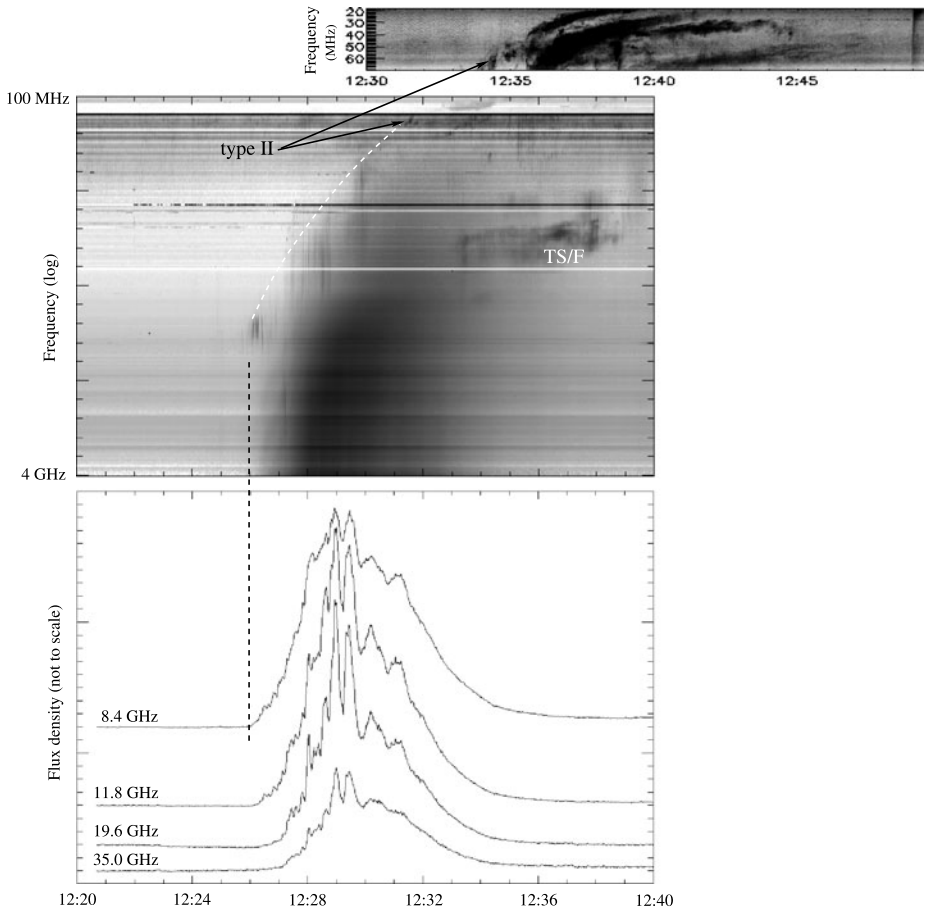


**Figure 5** Bumishus (8.4, 11.8, 19.6, and 35.0 GHz), ETHZ *Phoenix-2* (4 GHz–100 MHz), and GBSRBS (70–20 MHz) data on the 20 July 2004 event. Observations cover a wide radio frequency range between 20 MHz and 35 GHz. The dashed black vertical line points to the start of decimetric pulsations, with a simultaneous start of microwave emission. The white dashed line outlines the frequency-drifting pulsating structures, and black arrows point at the radio type II burst lanes (plasma emission at the fundamental; harmonics are also visible). ‘TS/F’ stands for emission that could be caused by a termination shock or a filament eruption; see text for details.

are expecting to see an upper–lower TS pair with no harmonic relation. The emission source locations at 410–432 MHz during 12:35–12:36 UT were marked with white ‘X’s in Figure 6. The locations appear west of the AR, in the same direction as the filament eruption observed by SOHO EIT, shown in Figure 2.

### 3. Analysis

#### 3.1. Periodicity Analysis

To find out periodicities in the observed radio data, we used the Fast Fourier Transform (FFT) method and Wavelet analysis, including the Global Wavelet Spectrum (GWS). The

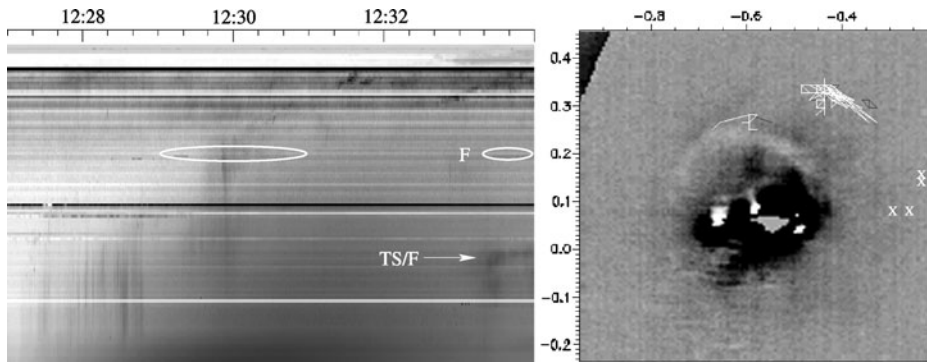


**Figure 6** Left: An extract of the ETHZ dynamic spectrum at 100–1200 MHz at 12:27–12:34 UT shows details of the pulsating decimetric structures. The range of the radio imaging at 12:29–12:31 UT at 410–432 MHz is indicated in the plot (white ellipse). The start of the termination shock/filament eruption ('TS/F') near 800 MHz and its possible fundamental emission near 400 MHz ('F') are also marked in the dynamic spectrum. (Note that Nançay has better sensitivity than the dynamic spectrum here, therefore sources not visible in the spectrum can still be imaged if the emission extends to the imaging frequencies.) Right: Locations of the pulsating radio source centers at 410 and 432 MHz during the 12:29–12:31 UT time period (white and black lines) plotted over the GOES SXI running difference image at 12:30 UT (reversed color scale, axis in units of solar radii). Source locations of the emission observed  $\sim$ 400 MHz during 12:35–12:36 UT are marked with white 'X's (possible termination shock/filament eruption, corresponding to the TS/F spectral feature).

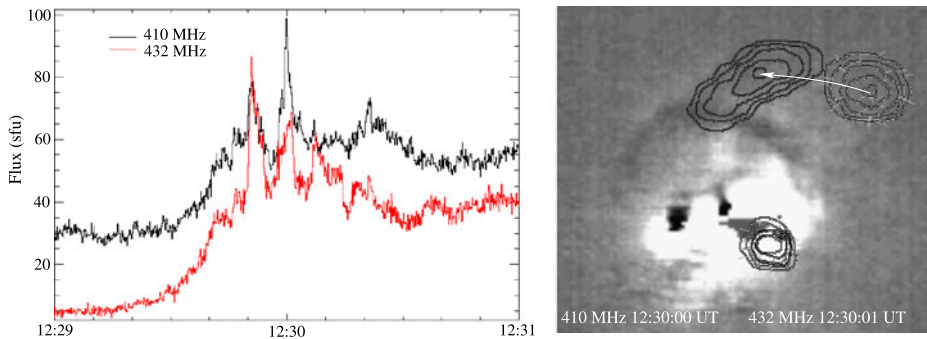


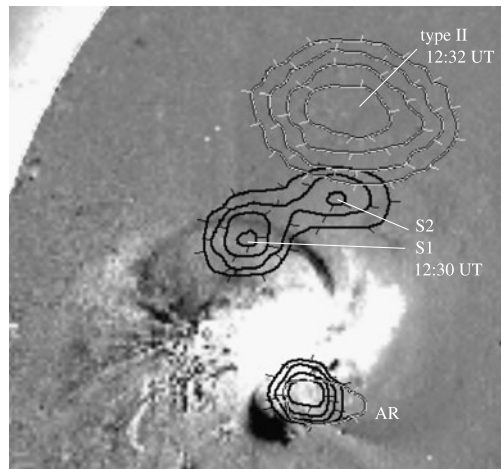
**Figure 7** Left: Flux density curves of the decimetric pulsations at 410 and 432 MHz during 12:29–12:31 UT. Some show evident frequency drifts toward the higher frequencies and some are non-drifting pulsations. Right: The frequency-drifting type III burst source at 12:30:00–12:30:01 UT has a horizontal trajectory toward the east (*Nançay Radioheliograph* imaging).

Morlet Wavelet (sixth order) was chosen to analyze the data (Torrence and Compo, 1998). These two different types of analysis can reveal both stationary and transient signals (global method, FFT) and long-lasting signals (local method, wavelet). In the FFT analysis we used different window functions for each data set from different instruments, in order to minimize the FFT response to noise (the level of noise and sampling rates were different for each instrument). A  $3\sigma$  significance level was used for listing the detected periods, where  $\sigma$  is the variance of the Fourier spectrum.

Bumishus flux density curves at four different frequencies were analyzed for the 12:26:40–12:28:40 UT period, which is the rising phase before the burst maximum. The



**Figure 8** A type II burst was formed above a pulsating decimetric radio source. The two pulsating sources are named S1 and S2 for the periodicity analysis. Black contours show the S1 and S2 source regions at 432 MHz at 12:30 UT, and grey contours show the type II burst region at 150 MHz at 12:32:52 UT. The background image is the EIT running difference image at 12:36 UT (note the time difference for the radio structures).



selected FFT window was  $[0, 20]$  s. The FFT power spectrum (Figure 9A) shows spectral peaks at 10 and 17 s for all the frequencies, but the  $3\sigma$  detection level is not exceeded by all. The spectral peaks at 8 s also fail to pass the  $3\sigma$  detection limits. The two lowest frequencies, 8.4 and 11.8 GHz, also show peaks at 14 and 13 s, respectively, unlike the other frequencies; see Table 1. Both frequencies are at the optically thick side of the flux spectrum, which might have effects on the emissivity.

*Phoenix-2* flux data in the 802–891 MHz range were analyzed for the 12:27:40–12:29:00 UT, 1600–1865 MHz range for the 12:23:50–12:26:30 UT, and 2500–3070 MHz range for the 12:27:00–12:27:30 UT periods, *i.e.*, during pulsations. The flux curves of four different *Phoenix-2* frequencies (802, 1690, 2620 and 3070 MHz) are plotted in Figure 9, together with their FFT spectra. The selected FFT window was  $[0, 30]$  s. The strongest periodicities are observed at 4, 8–12, and 14–16 s (Table 1).

**Table 1** Results from the Bumishus, *Phoenix-2* ETHZ, and *Nançay Radioheliograph* flux density data analysis: observing frequency, duration of the analyzed track, sampling frequency, and detected periodicity.

Frequency	Duration	$f_s$	Peak periods (FFT)	Periods (wavelet/GWS)
8.4 GHz	140 s	1 s	14, 17 s	12–16 s
11.8 GHz	140 s	1 s	10, 13, 17 s	7–13 s
19.6 GHz	140 s	1 s	11 s	8–13 s
35.0 GHz	140 s	1 s	10, 11, 17 s	8–12 s
802 MHz	110 s	0.1 s	6, 11, 14 s	6 and 10–18 s
1690 MHz	110 s	0.1 s	4, 8, 10, 12, 16 s	4 and 7–20 s
2620 MHz	30 s	0.1 s	7 s	3–5 and 7–9 s
3070 MHz	30 s	0.1 s	7 s	7–9 s
S1 <sup>a</sup>	120 s	150 ms	9, 11, 15 s	6–12 s
S2 <sup>b</sup>	120 s	150 ms	8, 9, 11, 15, 20 s	6–12 and 14–20 s

<sup>a</sup>Region S1:  $x = -0.75, -0.55$ ;  $y = 0.15, 0.50$  in units of solar radii, at 432 MHz.

<sup>b</sup>Region S2:  $x = -0.55, -0.20$ ;  $y = 0.15, 0.50$  in units of solar radii, at 432 MHz.

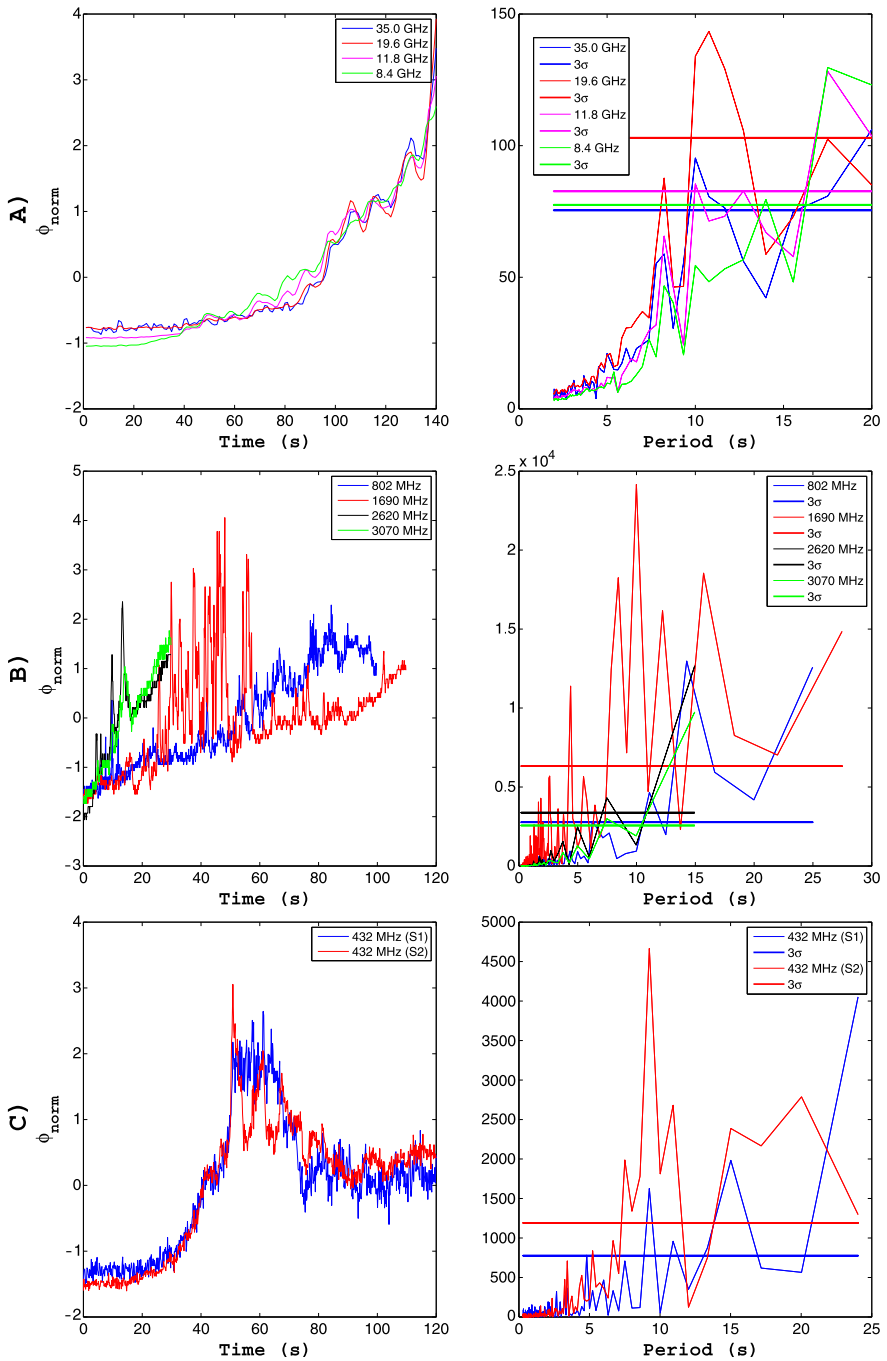


**Figure 9** FFT periodicity analysis with significance level  $3\sigma$ . Left: normalized flux density curves for (A) Bumishus flux curves at four fixed frequencies at microwaves; (B) examples of *Phoenix-2* flux curves at selected decimeter wave frequencies; (C) flux curves from the emission source regions S1 and S2, imaged with the *Nançay Radioheliograph* at 432 MHz. Right: their FFT spectra.

Periodicity analysis was also performed to the fluxes of the pulsating radio sources S1 and S2 that were imaged at 432 MHz (locations are shown in Figure 8). The FFT window was [0, 25], and the strongest detected periods are 9 and 15 s (Figure 9 and Table 1).

The wavelet analysis gave similar oscillation periods as the FFT analysis (Table 1). We did not use any strict confidence level in the wavelet analysis (GWS) because the analysis showed directly the oscillation period intervals. However, based on the wavelet analysis, it is difficult to define accurate spectral peak periods. The wavelet plots for the Bumishus 19.6 GHz flux, *Phoenix-2* 1690 MHz flux, and for the stronger S2 source flux are shown as examples in Figure 10.

Most of the analyzed flux curves show oscillation periods in the 8–12 s and 15–17 s range, and the wide or separate power spectral peaks indicate quasi-periodic pulsations. Oscillations of the imaged source regions S1 and S2 are similar to the high-frequency decimetric oscillations, which indicates that the acceleration processes were the same in both wavelength ranges.

### 3.2. Loop Oscillations

There can be several oscillation modes in coronal loops, with varying oscillation periods. The fast sausage mode is known to be the fastest MHD wave type. An estimate of the global sausage mode (GSM) period can be written as

$$\tau_{\text{GSM}} < \frac{2\pi a}{j_{0,s} v_{\text{AI}}} \approx \frac{2.62a}{v_{\text{AI}}}, \quad (1)$$

where  $v_{\text{AI}}$  is the Alfvén speed within the loop,  $j_{0,s}$  are the zeros from the Bessel function (2.4, 5.52, ...), and  $a$  is the loop cross section radius (Nakariakov, Melnikov, and Reznikova, 2003; Aschwanden, Nakariakov, and Melnikov, 2004). The values for the internal Alfvén speed (inside the loops) have usually been approximated as 1000–2000 km s<sup>-1</sup> (Aschwanden, 2003; Aschwanden, 2006; Pascoe, Nakariakov, and Arber, 2007), although for very long loops the Alfvén speed has been estimated to drop quite fast (Verwichte, Foullon, and Van Doorselaere, 2010).

There are speculations that the frequently used estimation of the fundamental fast sausage mode (FSM),  $\tau_{\text{FSM}} = 2\pi a/v_{\text{AI}}$  might be incorrect as only the higher harmonic nodes would satisfy the physical parameter requirements. Also, this estimation cannot be applied to the period of global sausage modes (Nakariakov, Melnikov, and Reznikova, 2003). Density plays a critical role in sausage mode oscillations and as the density is expected to vary within the loop, the detected periods may represent only partial loop segments (Aschwanden, 2006). For example, Aschwanden, Nakariakov, and Melnikov (2004) concluded that the oscillations are likely to be confined to a small segment near the apex of the flare loop, rather than involve the entire loop length.

The typical FSM oscillation periods in the solar corona have been estimated to vary between 0.1 and 10 s (Aschwanden, 2003; Aschwanden, 2006). Pascoe, Nakariakov, and Arber (2007) determined that for flaring coronal loops the global sausage modes (calculated using loop lengths) can vary between 5 and 60 s. Aschwanden *et al.* (1999) also calculated that for the typical parameters of EUV loops the mean FSM oscillation period is  $\approx 11$  s, with variations in the range of 3 to 44 s. The few existing radio imaging observations of oscillating coronal loops have shown periods in the 6–17 s range (Asai *et al.*, 2001; Nakariakov, Melnikov, and Reznikova, 2003).

In our case the cross section radius of the large overlying EUV loop was found to be  $\approx 4000$  km (5.5–6''; see Figure 1), and thus the calculated GSM oscillation period is about

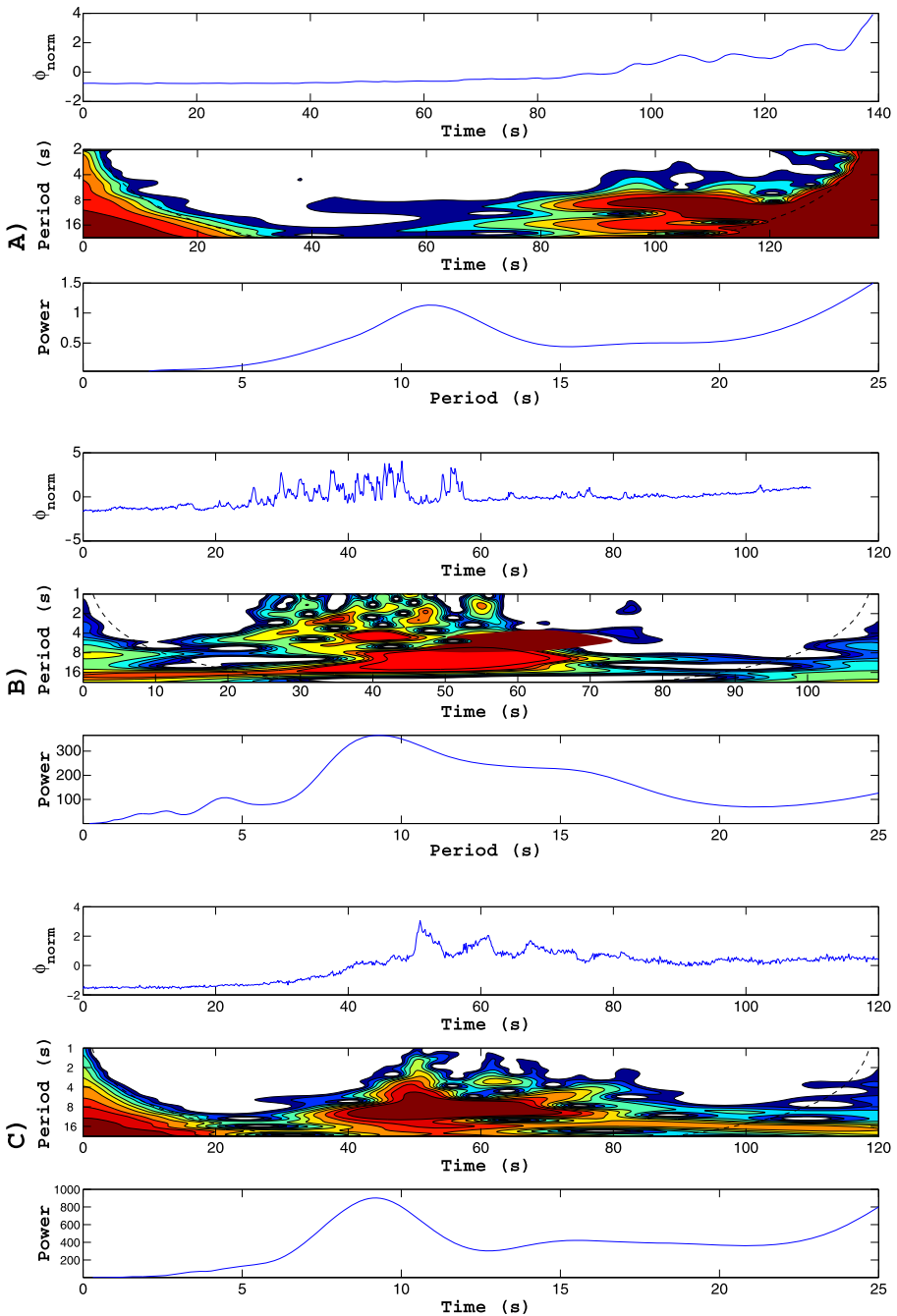


**Figure 10** Examples of wavelet analysis for the data sets presented in Figure 9: (A) Bumishus flux at 19.6 GHz; (B) Phoenix-2 flux at 1690 MHz; and (C) Nançay Radioheliograph emission source S2 flux at 432 MHz. The upper panel of each shows normalized data set. The middle panel of each shows global wavelet. The red color in the middle panel indicates strong oscillations and the blue color indicates weak oscillations.

10.5 s and the FSM fundamental period is about 25 s ( $v_{\text{AI}} = 1000 \text{ km s}^{-1}$ ; low density loop with estimated height of 120 000 km). The smaller loops located nearby (estimated heights  $\approx 40\,000 \text{ km}$ ) had more narrow widths, the cross section radii being about 1000 km (approximately  $1 - 1.5''$ ). Their GSM oscillation periods would then be about 2.6 s and the fundamental FSM periods about 6 s ( $v_{\text{AI}} = 1000 \text{ km s}^{-1}$ ).

The fast kink modes (FKM) are transverse loop oscillations and their global mode period is basically the Alfvén crossing time back and forth the loop length  $L$  (e.g., Aschwanden, 2006),

$$\tau_{\text{FKM}} = \frac{2L}{v_{\text{AI}}}. \quad (2)$$

We estimated the large EUV loop to have a length of about 270 000 km, thus giving an oscillation period of  $\sim 9$  minutes. The smaller EUV loops had lengths of about 100 000 km, which gives oscillation periods of  $\gtrsim 3$  minutes ( $v_{\text{AI}} = 1000 \text{ km s}^{-1}$ ).

We conclude that both GSM oscillations of the large overlying loop and first and second harmonic nodes of the FSM oscillations of the smaller nearby loops could produce the detected 8–12 s and 15–17 s oscillation periods.

The pulsating emission envelopes appeared in the spectrum at about 12:25:50, 12:27:20, and 12:29:20 UT, and the time separations between their starts were 90 and 120 s. For the first two envelopes we could determine their durations, which were approximately 60 and 90 seconds. These values are closest to the fast transverse (kink) modes of the smaller EUV loops.

### 3.3. Formation Heights and Propagation Speeds

The first pulsating envelope starting at 12:25:50 UT was observed in the 1.4–1.9 GHz range and the one starting at 12:29:20 UT in the 400–900 MHz range. If these emissions were formed by a propagating source, the frequency drift for the envelope was about  $4 \text{ MHz s}^{-1}$ . At 1.4 GHz plasma frequency the plasma density is about  $2.4 \times 10^{10} \text{ cm}^{-3}$  (plasma frequency  $f_p \approx 9000 \sqrt{n_e}$ ,  $n_e$  in  $\text{cm}^{-3}$ ) and at 400 MHz the density has decreased to  $2.0 \times 10^9 \text{ cm}^{-3}$ . Normally, atmospheric heights near the 400 MHz plasma frequency would not exceed 50 000 km. For comparison, the height of the large-scale EUV loop before contraction was about 120 000 km and the heights of the smaller nearby loops were  $\sim 40\,000 \text{ km}$ . It must be noted that the contraction of the overlying loop system could have reduced its atmospheric height to about 50 000 km. At 12:36 UT when contraction was first visible in the EIT image, the loop system could already have been rising and expanding, after the initial fast contraction phase.

In the dynamic spectrum, the type II burst start looks like a continuation of the pulsating emission envelopes. If we take the S2 pulsating source location at 432 MHz at 12:30:00 UT and compare it with the type II burst source location at 150 MHz at 12:32:52 UT, we get a (projected) spatial separation of about 80 000 km. If the driver of the pulsating emission source was the same for the type II shock, this would mean a driver speed of  $\sim 500 \text{ km s}^{-1}$ . Alternatively, we could use a high-density atmospheric model like ten times Saito (Saito, 1970) for the calculation of formation heights within the active region loop system (see, e.g., Pohjolainen *et al.*, 2007, for the different calculation techniques and the most commonly used atmospheric density models). Emission near 400 MHz would then be formed at height  $\sim 50\,000 \text{ km}$  and emission near 150 MHz at  $\sim 250\,000 \text{ km}$ , giving a distance separation of  $\sim 200\,000 \text{ km}$  and a speed of  $\sim 1200 \text{ km s}^{-1}$  between these two. Both speed estimates are realistic for a propagating coronal shock wave.

From the GBSRBS spectra at 70–20 MHz it is also possible to give rough estimates for the type II burst speeds. The faster-drifting emission lane at 12:36–12:38 UT shows a frequency drift of about  $0.1 \text{ MHz s}^{-1}$  and using standard atmospheric density models for the speed estimation we get speeds as high as  $1600\text{--}1900 \text{ km s}^{-1}$ . The slower-drifting emission lane has a drift of about  $0.05 \text{ MHz s}^{-1}$  and an estimated propagation speed of  $500\text{--}700 \text{ km s}^{-1}$ . This slower lane speed is in agreement with that calculated from the separation between the last pulsating features and the start of the type II burst.

#### 4. Results

The following results could be obtained from the data analysis:

- i) Loop contraction is observed in EUV. The collapse of loop height was detected in images taken after the quasi-periodic radio pulsations and after the flare impulsive phase. EUV image cadence was too poor to determine the start time or speed of contraction.
- ii)  $\text{H}\alpha$  and soft X-ray images show propagating bright patches and an arc-like bright front with dimmings behind it, respectively. These suggest that a propagating shock wave was formed during the flare impulsive phase.
- iii) After the radio pulsations in the flare impulsive phase, a slow-drifting spectral feature appeared which could be interpreted as reconnection outflow termination shock. However, it seemed to have fundamental–harmonic emission bands, unlike other reported TS features. This feature was located in almost opposite direction (west) compared to the contracting loop system (north-east).
- iv) Decimetric pulsations, inside frequency-drifting envelopes, show similar periodicities as observed in microwaves; the typical and most prevailing detected periods are within 8–12 and 15–17 s. The envelopes themselves appear 90 and 120 s apart, lasting for 60 and 90 s.
- v) The decimetric pulsating envelopes drift toward the lower frequencies. This suggests a rising electron acceleration site as the plasma density decreases. Microwave emission, with a typical gyrosynchrotron flux spectrum, is expected to rise from trapped electrons within the flare loop. As the periods of both the decimetric pulsations and the microwave oscillations are similar, we conclude that the electrons were created in the same acceleration process.
- vi) The decimetric pulsations form arc-like structures toward the north. The most pronounced pulsations (type III beams) were located in one region within the arc (marked S2 in Figure 8), above which a type II burst appeared soon after. Its observed location does not fit with a CME leading edge scenario. The appearance of the type II burst above the S2 pulsation region also suggests that the driver of the pulsating emission source could be the same as for the type II burst. The speed calculated from the time separation and distances match with the estimated type II burst speed.

#### 5. Discussion and Conclusions

Decimetric pulsations are generally believed to be caused by electrons trapped in flare loops, the view being supported by the often-observed temporal correlation with hard X-ray emission from the loop footpoints. Frequency-drifting, pulsating emission envelopes have been suggested to originate from electrons trapped in rising plasmoids or ejecta (*e.g.*, Kliem, Karlicky, and Benz, 2000; Khan *et al.*, 2002). However, in the event analyzed by Benz,

Battaglia, and Vilmer (2011), the emission source locations of the decimetric pulsations at different frequencies were in line and pointed to a coronal hard X-ray source, suggesting emission from a current sheet above the coronal source.

MHD oscillations have also been suggested to be the source of radio pulsations, especially in microwaves where the detected periods are short and reflect the flaring loop lengths. For example, spatially resolved microwave pulsations have been observed with well-defined periods of 14–17 s and 8–11 s (Melnikov *et al.*, 2005). The first, longer periods have been associated with global sausage modes within the flare loop, and the nodes at the footpoints. The shorter periodicities, however, could be associated with several different modes.

It has been proposed that coronal implosion, *i.e.*, contracting coronal loops, could be the exciter mechanism for loop oscillations. The analysis of Liu and Wang (2010) showed a two-stage evolution where the first slow contraction was followed by fast contraction, which lead to nearby loop oscillations with a period of about 10 minutes. Also in our event the calculated kink mode oscillations of the large overlying and contracting EUV loops produced periods of  $\sim 9$  minutes, while the smaller EUV loops nearby produced periods of  $\gtrsim 3$  minutes. However, these long periods were not detected in our radio data. On the other hand, fast kink mode oscillations of the shorter loops produced periods that are close to the time separation between the pulsating decimetric–metric emission envelopes (1.5–2 minutes). The calculated global and fast sausage modes of the large and smaller EUV loops were also short; in the range of 10–25 s and 2.6–6 s, respectively. As harmonic nodes are the most probable, fast sausage mode oscillations of the smaller EUV loops would match the observed periodicity in the radio emission.

Furthermore, Foullon *et al.* (2010) have suggested that the resonators of quasi-periodic pulsations may be large-scale but inner loops, instead of the background ‘quiet’ large loops (and subject to fast kink modes). They noted that the alternating left- and right-hand polarized decimetric emission could be due to the transverse motion of the loop, where the polarization changes with the period of the oscillating loop. However, Aschwanden (1986) pointed out that mildly polarized pulsations show a variable polarization versus frequency, which is probably due to propagation effects. This could be the case also in our event, where decimetric emission was only weakly polarized.

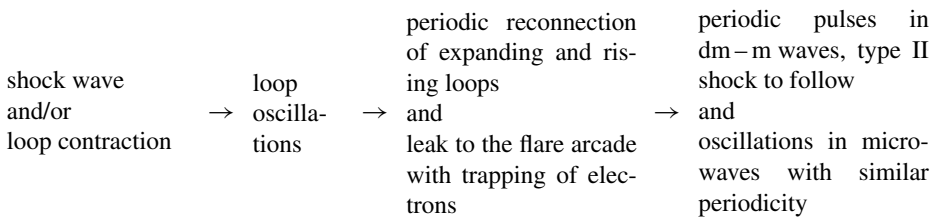
Our results, presented in Section 4, suggest a scenario similar to the one proposed by Nakariakov *et al.* (2006), where an oscillating loop situated nearby a flaring arcade is capable of leaking oscillations that modulate the current density and trigger magnetic reconnection. As MHD oscillation modes of a loop can interact with other structures located some distance away from the oscillating loop itself, the penetration depths can be quite large. The radio periodicity in our case could contain both long periods (pulse envelopes), created by the kink mode oscillations in the coronal loops, and short periods (periodic pulses) due to the fast sausage mode oscillations within the same loops. The accelerated particles would then be visible first near the acceleration sites as decimetric–metric pulses and soon after as trapped particles within the flare loop, emitting in microwaves.

Loop oscillations can be triggered by a wave (Aschwanden *et al.*, 1999) and the data suggest a wave was launched also in this event. Machado *et al.* (1988) noted that propagating soft X-ray fronts are linked with the brightening of remote H $\alpha$  patches and, in many cases, with radio type II emission. H $\alpha$  brightenings associated with a moving soft X-ray front have also been reported by, *e.g.*, Lehtinen *et al.* (2005). The most perceptible observation in our event is that the contracting large-scale EUV loops, the H $\alpha$  bright patches, the bright soft X-ray arc, the decimetric pulsations, and the type II burst all appear at locations close to each other, suggesting that these features are related.

Frequency-drifting, pulsating decimetric radio sources that are located in between the active region and the location of a later-appearing type II burst have earlier been reported by

Klassen, Pohjolainen, and Klein (2003). The pulsating structures were named type II *precursors* and they were observed above a large soft X-ray loop/wave front. Klassen, Pohjolainen, and Klein suggested that the flaring soft X-ray loops expanded into the overlying loops and then progressed through the loops by means of magnetic reconnection. This would have produced radio emission above the expanding loops, starting at continuously decreasing frequency as the reconnection gradually involved loops of decreasing electron density. In our event, the radio imaging of the pulsed decimetric – metric emission and the shock-generated radio type II burst indicate a similar close relationship between the two features. The observed radio emission locations, close to each other but in different direction compared to the erupting filament and the CME front, cannot be explained by the standard model of flare loops with above-located erupting plasmoid, driving a shock wave at the CME front.

Based on the observed emission characteristics, emission source locations, and the discussion above, we propose the following scenario for the eruption event:



The general validity of this scenario could be tested further with high time-cadence imaging in EUV (currently possible with the *Solar Dynamics Observatory*'s AIA instrument) and radio imaging at decimeter waves above 500 MHz (no instrumentation at present).

**Acknowledgements** We thank the research teams of all instruments, both satellite and ground-based, who have made their data available and easily accessible in the web archives. All ETHZ radio spectrometer data are available at <http://soleil.i4ds.ch/solarradio/>, and we thank Christian Monstein for useful comments and explanations on the ETHZ *Phoenix-2* data. The University of Bern radio polarimeters that were located at Bumishus in Switzerland are now at Tuorla Observatory in Finland and part of their data archive is available at the TUBE website at <http://tube.utu.fi/unibe-bursts/>. The radio monitoring survey at <http://secchirh.obsppm.fr/> is generated and maintained at the Observatoire de Paris by the LESIA UMR CNRS 8109, in cooperation with the Artemis team, Universities of Athens and Ioannina, and the Naval Research Laboratory. The *Green Bank Solar Radio Burst Spectrometer* (GBSRBS) is operated by the National Radio Astronomy Observatory, and the Global High Resolution H $\alpha$  Network is operated by the Space Weather Research Lab, New Jersey Institute of Technology. The GOES SXI data access system is a cooperative effort between NOAA's Space Weather Prediction Center (SWPC) and National Geophysical Data Center (NGDC). SOHO is a project of international cooperation between ESA and NASA, and TRACE was a NASA Small Explorer (SMEX) mission. The wavelet software was provided by C. Torrence and G. Compo, and it is available at <http://atoc.colorado.edu/research/wavelets/>.

## References

- Asai, A., Shimojo, M., Isobe, H., Morimoto, T., Yokoyama, T., Shibasaki, K., Nakajima, H.: 2001, *Astrophys. J. Lett.* **562**, L103.
- Aschwanden, M.J.: 1986, *Solar Phys.* **104**, 57.
- Aschwanden, M.J.: 2003, In: Erdélyi, R., Petrovay, K., Roberts, B., Aschwanden, M. (eds.) *Turbulence, Waves and Instabilities in the Solar Plasma*, Kluwer Academic, Dordrecht, 215.
- Aschwanden, M.J.: 2006, *Roy. Soc. Lond. Philos. Trans. Ser. A* **364**, 417.
- Aschwanden, M.J., Fletcher, L., Schrijver, C.J., Alexander, D.: 1999, *Astrophys. J.* **520**, 880.
- Aschwanden, M.J., Nakariakov, V.M., Melnikov, V.F.: 2004, *Astrophys. J.* **600**, 458.
- Aurass, H., Mann, G.: 2004, *Astron. Astrophys.* **615**, 526.
- Benz, A.O., Battaglia, M., Vilmer, N.: 2011, *Solar Phys.* **273**, 363.



- Dulk, G.A.: 1985, *Ann. Rev. Astron. Astrophys.* **23**, 169.
- Foullon, C., Fletcher, L., Hannah, I.G., Verwichte, E., Cecconi, B., Nakariakov, V.M., Phillips, K.J.H., Tan, B.L.: 2010, *Astrophys. J.* **719**, 151.
- Grechnev, V.V., White, S.M., Kundu, M.R.: 2003, *Astrophys. J.* **588**, 1163.
- Ji, H., Huang, G., Wang, H.: 2007, *Astrophys. J.* **660**, 893.
- Karlicky, M.: 2004, *Astron. Astrophys.* **417**, 325.
- Karlicky, M., Kosugi, T.: 2004, *Astron. Astrophys.* **419**, 1159.
- Khan, J.I., Vilmer, N., Saint-Hilaire, P., Benz, A.O.: 2002, *Astron. Astrophys.* **388**, 363.
- Klassen, A., Pohjolainen, S., Klein, K.-L.: 2003, *Solar Phys.* **218**, 197.
- Kliem, B., Karlicky, M., Benz, A.O.: 2000, *Astron. Astrophys.* **360**, 715.
- Lehtinen, N.J., Pohjolainen, S., Karlicky, M., Aurass, H., Otruba, W.: 2005, *Astron. Astrophys.* **442**, 1049.
- Liu, R., Wang, H.: 2009, *Astrophys. J. Lett.* **703**, L23.
- Liu, R., Wang, H.: 2010, *Astrophys. J. Lett.* **714**, L41.
- Liu, R., Wang, H., Alexander, D.: 2009, *Astrophys. J.* **696**, 121.
- Machado, M.E., Xiao, Y.C., Wu, S.T., Prokakis, Th., Dialetis, D.: 1988, *Astrophys. J.* **326**, 451.
- Melnikov, V.F., Reznikova, V.E., Shibasaki, K., Nakariakov, V.M.: 2005, *Astron. Astrophys.* **439**, 727.
- Nakariakov, V.M., Foullon, C., Verwichte, E., Young, N.P.: 2006, *Astron. Astrophys.* **452**, 343.
- Nakariakov, V.M., Melnikov, V.F., Reznikova, V.E.: 2003, *Astron. Astrophys.* **412**, L7.
- Pascoe, D.J., Nakariakov, V.M., Arber, T.D.: 2007, *Astron. Astrophys.* **461**, 1149.
- Pohjolainen, S., van Driel-Gesztelyi, L., Culhane, J.L., Manoharan, P.K., Elliott, H.A.: 2007, *Solar Phys.* **244**, 167.
- Saito, K.: 1970, *Ann. Tokyo Astron. Obs.* **12**, 53.
- Torrence, C., Compo, G.P.: 1998, *Bull. Am. Meteorol. Soc.* **79**, 61.
- Verwichte, E., Foullon, C., Van Doorselaere, T.: 2010, *Astrophys. J.* **717**, 458.
- White, S.M.: 2007, *Asian J. Phys.* **16**, 189.